Saturation Mechanism of Decaying Ion Temperature Gradient Driven Turbulence with Kinetic Electrons*)

Yasuhiro IDOMURA

Japan Atomic Energy Agency, 178-4 Wakashiba, Kashiwa, Chiba 277-0871, Japan

(Received 5 November 2015 / Accepted 7 December 2015)

We present full-f gyrokinetic simulations of the ion temperature gradient driven (ITG) turbulence including kinetic electrons. By comparing decaying ITG turbulence simulations with adiabatic and kinetic electron models, an impact of kinetic electrons on the ITG turbulence is investigated. It is found that significant electron transport occurs even in the ITG turbulence, and both ion and electron temperature profiles are relaxed. In steady states, both cases show upshifts of nonlinear critical ion temperature gradients from linear ones, while their saturation mechanisms are qualitatively different. In the adiabatic electron case, the ITG mode is stabilized by turbulence driven zonal flows. On the other hand, in the kinetic electron case, passing electrons transport shows fine resonant structures at mode rational surfaces, which generate corrugated density profiles. Such corrugated density profiles lead to fine radial electric fields following the neoclassical force balance relation. The resulting $E \times B$ shearing rate greatly exceeds the linear growth rate of the ITG mode.

Keywords: full-f gyrokinetic model, ion temperature gradient driven turbulence, kinetic electron

DOI: 10.1585/pfr.11.2403006

1. Introduction

In full-f gyrokinetic simulations [1], the total particle distribution f including both a macroscopic equilibrium distribution f_0 and a microscopic turbulent perturbation δf is evolved following turbulent and collisional transport processes described by a single Fokker-Planck equation. Thanks to the multi-scale and multi-physics properties, full-f gyrokinetic simulations disclosed rich physics such as self-organized critical phenomena in avalanche-like non-local transport, turbulence regulation by mean flows or radial electric fields given by the neoclassical radial force balance relation, and intrinsic rotation induced by non-diffusive momentum transport [2–4]. In addition, with increasing computing power, validation studies on transport scalings with respect to the plasma size, the collisionality, and the heating power were enabled, and qualitative features of experimental transport scalings were recovered [5–7]. Although applications of full-f gyrokinetic simulations have been greatly expanded, their electron model has been limited to adiabatic electrons, and electron transport in full-f gyrokinetic simulations has been an open issue for a long time. In order to resolve this critical issue, we developed a new hybrid kinetic electron model for electrostatic full-f gyrokinetic simulations [8]. In the model, we apply a full kinetic electron model to the gyrokinetic equation with the multi-species linear Fokker-Planck collision operator. On the other hand, in the gyrokinetic Poisson equation, non-axisymmetric turbulent fluctuations are computed using trapped kinetic electrons responses, while axisymmetric radial electric fields are determined using full kinetic electrons responses. By taking this approach, one can avoid the so-called ω_H mode [9] or a high frequency mode with $\omega_H \sim \Omega_i$, which is unphysical from the viewpoint of the gyrokinetic ordering $\omega \ll \Omega_i$, while keeping important physics such as the ion temperature gradient driven trapped electron mode (ITG-TEM) turbulence and the neoclassical transport with the ambipolar condition. The model was implemented on the full-f gyrokinetic Eulerian code GT5D [2, 10], and full-f gyrokinetic simulations with kinetic electrons were enabled with a reasonable computational cost.

In this work, we present decaying ITG turbulence simulations with kinetic electrons and discuss influences of kinetic electrons on the saturation mechanism of the ITG turbulence. It is well known that the growth rate of the ITG mode is increased by kinetic electrons, because adiabatic electrons responses are reduced in the presence of trapped electrons. Kinetic electrons responses induce particle transport, which has complicated pinch and transport characteristics depending on dominant modes [11]. In addition, recent δf flux-tube simulations reported that significant electron transport is induced by passing electrons in the vicinity of mode rational surfaces [12]. Unlike fixed gradient δf simulations, in full-f gyrokinetic simulations, this kind of localized electron transport may lead to local change of density and electron temperature profiles, which are connected with radial electric fields in a self-consistent manner. Therefore, it is of great interest to investigate an impact of such a feedback on the saturation mechanism.

author's e-mail: idomura.yasuhiro@jaea.go.jp

*) This article is based on the presentation at the 25th International Toki Conference (ITC25).

The reminder of the paper is organized as follows. In Sec.2, the multi-species full-f gyrokinetic equations with the hybrid kinetic electron model are presented. In Sec.3, influences of kinetic electrons are discussed by comparing decaying ITG turbulence simulations with kinetic and adiabatic electrons. Finally, a summary is given in Sec.4.

2. Calculation Model

We consider electrostatic micro-turbulence in an axisymmetric tokamak configuration. GT5D solves the following gyrokinetic equation [13],

$$\frac{\partial f_s}{\partial t} + \dot{\mathbf{R}} \cdot \frac{\partial f_s}{\partial \mathbf{R}} + \dot{v}_\parallel \frac{\partial f_s}{\partial v_\parallel} = \sum_{s'} C(f_s, f_{s'}) + S_{src,s}, \quad (1)$$

$$\dot{\mathbf{R}} = v_\parallel \mathbf{b} + \frac{c}{q_s B_\parallel^*}\mathbf{b} \times \left(q_s \nabla \langle \phi \rangle_s + m_s v_\parallel^2 \mathbf{b}\cdot\nabla\mathbf{b} + \mu \nabla B \right), \quad (2)$$

$$\dot{v}_\parallel = -\frac{\mathbf{B}^*}{m_s B_\parallel^*} \cdot (q_s \nabla \langle \phi \rangle_s + \mu \nabla B), \quad (3)$$

in the gyro-center coordinates $\mathbf{Z} = (t; \mathbf{R}, v_\parallel, \mu, \alpha)$. Here, f_s denotes the guiding-center distribution function of the particle species s, $C(f_s, f_{s'})$ is a multi-species Coulomb collision operator, $S_{src,s}$ is a source term, $\mathbf{R}$ is the position of the guiding center, $\mathbf{v}$ is the velocity of the guiding center, $v_\parallel = \mathbf{b}\cdot\mathbf{v}$ and $v_\perp = |\mathbf{b}\times\mathbf{v}|$ are the velocities in the parallel and perpendicular direction to the magnetic field, $\mu = m_s v_\perp^2/2B$ is the magnetic moment, α is the gyro-phase angle, $\mathbf{B} = B\mathbf{b}$ is the magnetic field, $\mathbf{b}$ is the unit vector in the parallel direction, m_s and q_s are the mass and charge, respectively, c is the velocity of light, $\Omega_s = q_s B/m_s c$ is the cyclotron frequency, $B_\parallel^* = \mathbf{b}\cdot\mathbf{B}^*$ is a parallel component of $\mathbf{B}^* = \mathbf{B} + (B v_\parallel/\Omega_s)\nabla\times\mathbf{b}$, ϕ is the electrostatic potential of turbulent fields, and the gyro-averaging operator is defined as $\langle\cdot\rangle_s \equiv \oint \cdot d\alpha/2\pi$. The multi-species collision operator is given by the zeroth order equipartition operator and the linear Fokker-Planck collision operator [14]. The former is essential in full-f approaches, in which an equilibrium distribution of each species may have different temperature at each time step, and the resulting interaction between multiple transport channels through the equipartition process affects relative importance of each transport channel and the total power balance.

The self-consistency is imposed by the gyrokinetic Poisson equation or the quasineutrality condition, $\sum_s q_s \delta n_s = 0$, where the perturbed density δn_s is defined with respect to the initial density n_{s0} satisfying $\sum_s q_s n_{s0} = 0$. In this work, we define the ion density using a linear polarization density with a long wavelength approximation, $k_\perp^2 \rho_{ti}^2 \ll 1$,

$$\delta n_i = \int \delta f_i \delta([\mathbf{R}+\rho] - \mathbf{x}) d^6 Z + \frac{1}{4\pi q_i} \nabla_\perp \cdot \frac{\rho_{ti}^2}{\lambda_{Di}^2} \nabla_\perp \phi, \quad (4)$$

where δf_s is the perturbed distribution defined against the initial distribution f_{s0}, $\mathbf{R}+\rho$ is the particle position, $\rho = \mathbf{b}\times\mathbf{v}/\Omega_s$ is the Larmor radius, $d^6Z = m_s^2 B_\parallel^* d\mathbf{R} dv_\parallel d\mu d\alpha$ is the phase space volume of the gyro-center coordinates, $\rho_{ts} = v_{ts}/\Omega_s$ is the Larmor radius evaluated with the thermal velocity $v_{ts} = (T_s/m_s)^{1/2}$, $\lambda_{Ds} = (T_s/4\pi n_s q_s^2)^{1/2}$ is the Debye length.

The perturbed electron density is computed using a hybrid kinetic electron model [8]. In this model, we solve the full-f gyrokinetic equation (1) using a full kinetic electron model including both trapped and passing electrons. This treatment enables us to compute collisional processes and thus the neoclassical transport. In nonlinear simulations, this treatment also describes trapping and detrapping processes due to the parallel nonlinearity and the radial transport of electrons between magnetic surfaces with different local aspect ratios and thus trapped-passing boundaries. We use only the perturbed density of trapped electrons for calculating the electrostatic potential of finite n modes, while the radial electric field E_r is computed using the perturbed density of both trapped and passing electrons. This treatment is essential for eliminating the ω_H mode with keeping the ambipolar condition. Since the ambipolar condition is connected with the toroidal angular momentum conservation, this feature is of critical importance for computing toroidal rotation. In computing E_r, we neglect $m \neq 0$ components, which have finite $k_\parallel$ and are subject to the ω_H mode. Here, m and n denote the poloidal and toroidal mode numbers. This approximation changes the eigenfrequency of geodesic acoustic modes (GAMs), while the residual zonal flows are not affected. In Ref. [8], it was shown that this approximation gives a minor effect on the ITG turbulence at far above critical temperature gradients, where linear damping effects of zonal flows are subdominant compared with nonlinear ones [6]. The resulting kinetic electron density is defined as

$$\delta n_{e,n\neq 0} = \int \delta f_{e,t,n\neq 0} \delta([\mathbf{R}+\rho] - \mathbf{x}) d^6 Z - \alpha_p n_e \frac{q_e \phi_{n\neq 0}}{T_e}, \quad (5)$$

$$\delta n_{e,n=0} = \int \delta f_{e,n=0} \delta([\mathbf{R}+\rho] - \mathbf{x}) d^6 Z, \quad (6)$$

where the second term of Eq. (5) denotes an adiabatic passing electrons response, and α_p is the flux-surface averaged fraction of passing electrons. The perturbed electron distribution is decomposed into trapped and passing components, $\delta f_e = \delta f_{e,t} + \delta f_{e,p}$, which are defined by contributions from velocity space grids satisfying $\frac{1}{2} m_e v_\parallel^2 + \mu B > \mu B_{max}$ and $\frac{1}{2} m_e v_\parallel^2 + \mu B < \mu B_{max}$, respectively. Here, B_{max} is the maximum magnetic field of the magnetic surface, on which the velocity space grid is defined. The above hybrid kinetic electron model successfully eliminates the ω_H mode with keeping important physical effects in full-f gyrokinetic simulations, such as the ITG-TEM turbulence, the neoclassical transport, the ambipolar condition, particle trapping and de-trapping processes, and passing elec-

trons transport due to passive responses to turbulent fluctuations. Detailed verification tests on conservation properties, neoclassical transport, zonal flow damping, and linear ITG-TEM calculations were reported in Ref. [8].

3. Decaying ITG Turbulence Simulations

In this work, we consider deuterium plasmas in a circular concentric tokamak configuration with $R_0/a = 2.79$, $a/\rho_{ti} = 150$, and $q(r) = 0.85 + 2.18(r/a)^2$, which has the following Cyclone like parameters [15] at $r_s = 0.5a$: $\epsilon = r_s/R \sim 0.18$, $q(r_s) \sim 1.4$, $\hat{s}(r_s) = [(r/q)dq/dr]_{r=r_s} \sim 0.78$, $n_e \sim 4.6 \times 10^{19}\mathrm{m}^{-3}$, $R_0/L_n = 2.22$, $T_e \sim T_i \sim 2\mathrm{keV}$, $R_0/L_{te} = R_0/L_{ti} = 6.92$. Here, r is the radial coordinate, q is the safety factor, ϵ is the local inverse aspect ratio, n_e is the electron density, T_e and T_i are the electron and ion temperature, L_n, L_{te}, and L_{ti} are the corresponding scale lengths, and the initial distribution f_{s0} is given by a local Maxwellian distribution. We use the hybrid electron model with the mass ratio of $m_i/m_e = 100$. The normalized electron and ion collisionality parameters at $r = r_s$ are $\nu_{*e} = (4/3\sqrt{\pi})qR_0\hat{\nu}_{ei}/v_{te}\epsilon^{3/2} \sim 0.034$ and $\nu_{*i} = (2\sqrt{2}/3\sqrt{\pi})qR_0\hat{\nu}_{ii}/v_{ti}\epsilon^{3/2} \sim 0.024$, respectively. It is noted that ν_{*e} and thus electron neoclassical transport properties are not affected by the heavy electron model. In the decaying ITG turbulence simulation, we impose no source term, while a Krook type sink operator is used to impose a L-mode like fixed boundary condition with $n_e \sim 4 \times 10^{19}\mathrm{m}^{-3}$, $U_e = U_i = 0$, and $T_e = T_i \sim 1\,\mathrm{keV}$. The particle and energy fluxes are defined as $\Gamma_s \equiv \langle f_s\dot{\mathbf{R}} \cdot \nabla r\rangle_{gf}$ and $Q_s \equiv \langle[m_s v_\parallel^2/2 + \mu B]f_s\dot{\mathbf{R}} \cdot \nabla r\rangle_{gf}$, where the gyro/flux-surface average operator is defined as $\langle A\rangle_{gf} \equiv \langle\int A(\mathbf{Z})\delta(\mathbf{R} + \rho - \mathbf{x})d^6Z\rangle_f$ and $\langle\cdot\rangle_f$ is the flux-surface average operator. From convergence tests in Ref. [8], we have chosen numerical parameters as $(N_R, N_\zeta, N_Z, N_{v\parallel}, N_\mu) = (160, 32, 160, 96, 20)$ with 1/6 wedge torus model ($n = 0, 6, \cdots, 48$ or $k_\theta(r_s)\rho_{ti} = 0 \sim 0.9$), and $\Delta_t = 2\Omega_i^{-1}$.

Figure 1 shows linear growth rate spectra of the ITG-TEM. With kinetic electrons, a transition between the ITG mode to the TEM occurs at $R/L_{ti} \sim 5.5$ in the collisionless case, and there is no critical L_{ti}. Although the transition occurs at lower R/L_{te} in the collisional case, this feature is unchanged. In the case with $L_{te} = L_{ti}$, the TEM is stabilized at lower R/L_{te}, and one can identify a critical L_{ti} of the ITG mode at $R/L_{ti} \sim 3.3$, which is lower than that with adiabatic electrons, $R/L_{ti} \sim 4$. The present decaying turbulence simulations are initialized at far above these linear critical gradients, and dominated by the ITG mode.

Figures 2 and 3 show the time histories of the energy fluxes and the temperature gradients. In decaying turbulence simulations, the ITG mode is excited from the linearly unstable initial condition, and the temperature profile is relaxed towards the steady state at a nonlinear critical gradient, where turbulent transport is quenched. In contrast to the adiabatic electron case, where electron transport is

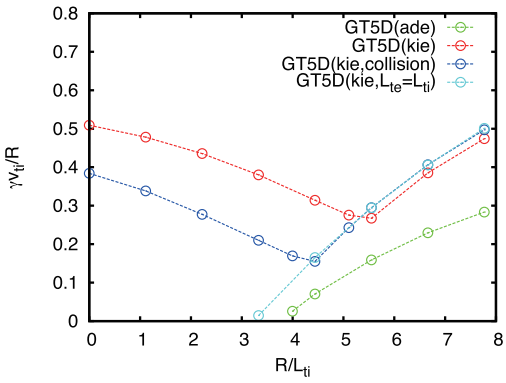

Fig. 1 The L_{ti} dependency of linear growth rate spectra at $k_\theta\rho_{ti} \sim 0.28$. The adiabatic electron result (ade) and kinetic electron results with (kie, collision) and without collisions (kie) are compared. Except for the case with $L_{te} = L_{ti}$, L_{te} is fixed at $R/L_{te} = 6.92$.

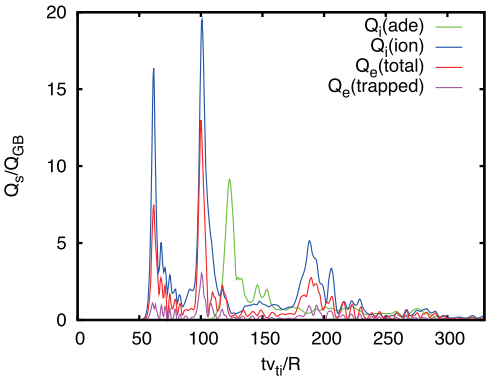

Fig. 2 The time history of the energy fluxes, Q_e and Q_i, averaged over $r/a = 0.4 \sim 0.6$. In the kinetic electron case, a trapped particle fraction of Q_e is also shown.

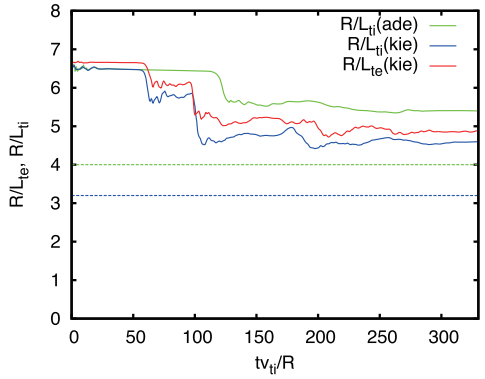

Fig. 3 The time history of R/L_{te} and R/L_{ti} averaged over $r/a = 0.4 \sim 0.6$. Green and blue broken lines show linear critical L_{ti} for the adiabatic and kinetic electron cases, respectively.

neglected, the kinetic electron case shows significant electron transport even in the ITG dominant parameter. In addition, a significant fraction of the electron energy flux is

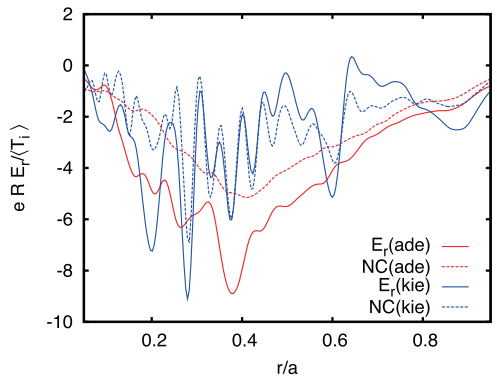

Fig. 4 The radial electric fields in the final state of the decaying ITG turbulence simulations. Broken lines show estimations with the neoclassical force balance relation.

induced by passing electrons transport. Since the magnetic drifts give opposite toroidal resonance conditions between ions and electrons, this passing electrons response is attributed to slab like resonance conditions due to passing motion. The resulting temperature relaxation occurs both for ions and electrons, and the final R/L_{ti} is lower than that with adiabatic electrons. In both cases, the nonlinear critical temperature gradients exhibit significant upshifts from the linear ones. In the adiabatic electron case, this phenomenon is well known as the so-called Dimits shift, where the ITG mode is suppressed by turbulence driven zonal flows. However, in the kinetic electron case, the saturation mechanism is different from the Dimits shift.

Figures 4 and 5 shows the radial electric fields E_r and the corresponding $E \times B$ shearing rates $\omega_{E\times B}$ observed in the final steady state. Although global structures in both cases follow the neoclassical force balance relation [16], their fine structures are significantly different. In the adiabatic electron case, the $E \times B$ shearing rate with $\omega_{E\times B} \sim \gamma$ is produced in the plasma core, and its radial profile is largely deviated from the neoclassical force balance relation. Therefore, the fine E_r structures are attributed to the turbulence driven (residual) zonal flows. On the other hand, in the kinetic electron case, the fine E_r structures with $\omega_{E\times B} \gg \gamma$ are almost determined by the radial force balance relation. Here, the dominant contribution is coming from the density gradient. Therefore, the key physics in the kinetic electron case is particle transport and the resulting density profiles.

In Fig. 6, the final density profile shows slight global peaking and radially corrugated fine structures, which are consistent with particle transport in Fig. 7. The particle transport is characterized by trapped electrons global inward pinch and passing electrons transport. The trapped electrons inward pinch may be consistent with the turbulent equipartition (TEP) theory [17, 18] or a curvature drift pinch [11]. On the other hand, the passing electrons outward transport shows fine resonant structures at mode rational surfaces, where passing electrons satisfy a resonance condition $\omega/k_\parallel \sim v_{te}$. This structure becomes finer and then continuous towards the outer region reflecting the density of mode rational surfaces. In contrast to zonal flow structures, which are determined by various nonlinear dynamics [19], the fine E_r structure is determined mostly by linear resonance conditions given by the q profile. Therefore, this saturation mechanism is qualitatively different from the Dimits shift.

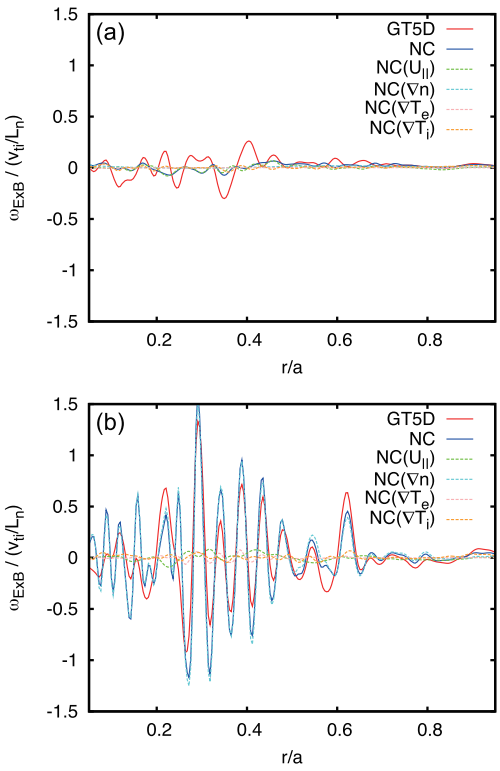

Fig. 5 The $E \times B$ shearing rates in the final state of the decaying ITG turbulence simulations with (a) adiabatic electrons and (b) kinetic electrons. Also plotted are estimations with the neoclassical force balance relation, and contributions from parallel flows, density gradients, and temperature gradients.

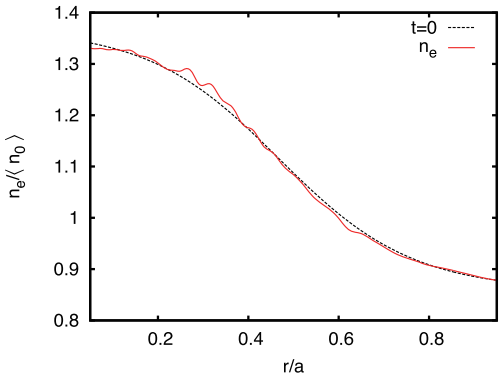

Fig. 6 The density profile in the final state of the decaying ITG turbulence simulations with kinetic electrons. A broken line shows the initial condition.

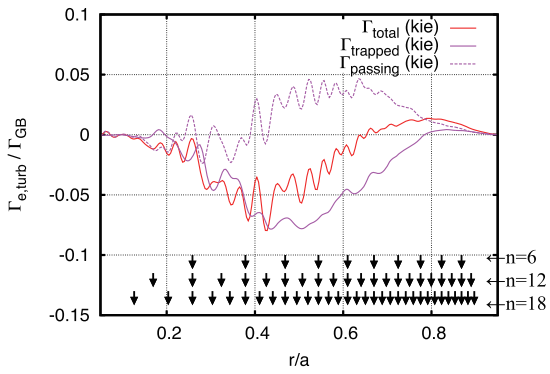

Fig. 7 The particle fluxes averaged over $tv_{ti}/R = 50 \sim 340$. A red line shows the total flux, while solid and broken magenta lines are trapped and passing fractions, respectively. Arrows indicate positions of mode rational surfaces satisfying $q(r) = m/n$ for each n.

4. Summary

In this work, we have investigated influences of kinetic electrons on decaying ITG turbulence using GT5D with the hybrid kinetic electron model. It is found that with kinetic electrons, significant electron transport occurs even in the ITG turbulence, and both ion and electron temperature profiles are relaxed. In the steady state, upshifts of nonlinear critical ion temperature gradients from linear ones are observed both for the adiabatic and kinetic electron cases, while the latter gives lower critical R/L_{ti}. In the former, turbulence driven zonal flows suppress the ITG mode, which is consistent with the Dimits shift picture. On the other hand, in the latter, passing electrons transport shows fine resonant structures, which generate corrugated density profiles. Such corrugated density profiles lead to fine radial electric fields following the neoclassical force balance relation. The resulting $E \times B$ shearing rate greatly exceeds the linear growth rate of the ITG mode. Although fine E_r structures are generated in both cases, their mechanisms are qualitatively different. The former is characterized by nonlinear turbulence dynamics, while the latter is mostly determined by linear resonance structures given by the magnetic configuration. In the future work, we will investigate how the above saturation mechanism affect profile stiffness in fixed flux ITG turbulence simulations.

Acknowledgments

The computation in this work was performed on the BX900 at the JAEA, the Helios at the IFERC, the FX10 at the Univ. Tokyo, and the K-computer (hp150027) at the Riken. This work is supported by the MEXT, Grant for HPCI Strategic Program Field No.4: Next-Generation Industrial Innovations, Grant for Post-K priority issue No.6: Development of Innovative Clean Energy, and Grant No. 22686086.

[1] Y. Idomura, M. Nakata and S. Jolliet, Plasma Fusion Res. **9**, 3503028 (2014).
[2] Y. Idomura, H. Urano, N. Aiba and S. Tokuda, Nucl. Fusion **49**, 065029 (2009).
[3] Y. Idomura, Computational Science and Discovery **5**, 014018 (2012).
[4] Y. Idomura, Phys. Plasmas **21**, 022517 (2014).
[5] S. Jolliet and Y. Idomura, Nucl. Fusion **52**, 023026 (2012).
[6] M. Nakata and Y. Idomura, Nucl. Fusion **53**, 113039 (2013).
[7] Y. Idomura and M. Nakata, Phys. Plasmas **21**, 020706 (2014).
[8] Y. Idomura, submitted to J. Comput. Phys.
[9] W.W. Lee, J. Comput. Phys. **72**, 243 (1987).
[10] Y. Idomura, M. Ida, T. Kano, N. Aiba and S. Tokuda, Comput. Phys. Commun. **179**, 391 (2008).
[11] C. Bourdelle, X. Garbet, F. Imbeaux, A. Casati, N. Dubuit, R. Guirlet and T. Parisot, Phys. Plasmas **14**, 112501 (2007).
[12] J. Dominski, S. Brunner, T. Gorler, F. Jenko, D. Told and L. Villard, Phys. Plasmas **22**, 062303 (2015).
[13] A.J. Brizard and T.S. Hahm, Rev. Mod. Phys. **79**, 421 (2007).
[14] H. Sugama, T.-H. Watanabe and M. Nunami, Phys. Plasmas **16**, 112503 (2009).
[15] A.M. Dimits, G. Bateman, M.A. Beer, B.I. Cohen, W. Dorland, G.W. Hammett, C. Kim, J.E. Kinsey, M. Kotschenreuther, A.H. Kritz, L.L. Lao, J. Mandrekas, W.M. Nevins, S.E. Parker, A.J. Redd, D.E. Shumaker, R. Sydora and J. Weiland, Phys. Plasmas **7**, 969 (2000).
[16] S.P. Hirshman and D.J. Sigmar, Nucl. Fusion **21**, 1079 (1981).
[17] M.B. Isichenko, A.V. Gruzinov and P.H. Diamond, Phys. Rev. Lett. **74**, 4436 (1995).
[18] X. Garbet, L. Garzotti, P. Mantica, H. Nordman, M. Valovic, H. Weisen and C. Angioni, Phys. Rev. Lett. **91**, 035001 (2003).
[19] P.H. Diamond, S.-I. Itoh, K. Itoh and T.S. Hahm, Plasma Phys. Control. Fusion **47**, R35 (2005).